445 Wozniak and Anderson (73), released HGF may induce c-met expression as an
446 immediate-early gene, thus also enhance HGF-c-met signaling in the satellite cell activation
447 process. They additionally observed that the level of satellite cell activation was increased
448 in un-stretched fibers from mdx and nNOS-knockout mice and in un-stretched normal fibers
449 by treatment with a competitive NOS-inhibitor L-NAME (N^G-nitro-L-arginine methylester),
450 suggesting that a NO-independent HGF/c-met signaling pathway, and possibly other
451 signaling pathways, control activation in muscle deficient in dystrophin and nNOS (73).
452 It has not been determined how quiescent satellite cells sense mechanical stimuli to
453 generate biochemical signals that elevate intracellular calcium ion concentrations; therefore,
454 in the present work, the involvement of MS- and VGC-channels in the
455 mechano-transduction system was examined. When satellite cell cultures were incubated
456 with the MS-channel inhibitor GsMTx-4, the L-VGC-channel inhibitor nifedipine, or a less
457 specific inhibitor, gadolinium chloride, stretch-induced HGF release from the matrix and the
458 resulting cell activation were abolished completely in a dose-dependent manner. This was
459 revealed by western blotting of conditioned media and a BrdU-incorporation assay (Fig. 2).
460 By contrast, the T- VGC-channel inhibitor NNC55-0396 did not have inhibitory effects on
461 the activation index. Addition of the calcium-chelator EGTA to culture media also
462 inhibited the stretch-activation response and HGF release, indicating the significance of
463 extracellular calcium ions in the activation cascade (Fig. 1 and Fig. 2 panel *B*). This
464 means that free calcium ions stored in mitochondria may now be excluded from a role in
465 this activation pathway. Calcium-imaging analyses verified these results, and therefore
466 provide direct evidence that both MS- and L-VGC-channels are essential in calcium ion
467 influx in response to mechanical stretch and that calcium ions may flow in through
468 L-VGC-channels (Fig. 4). A possible explanation for these observations can be addressed
469 by a possible model of MS-/L-VGC-channel coupling, in which the MS-channel responds
470 to mechanical stimuli by gating cations; this would result in local depolarization of the
471 plasma membrane, a signal that is then quickly sensed by L-VGC-channels ($Ca_{v1.1}$, $Ca_{v1.2}$)
472 that allow a significant amount of calcium ions to permeate the cell and lead to
473 calcium-calmodulin formation (see Fig. 5 panel *B* for details). In the nifedipine treatment,
474 in which MS-channels are expected to retain biological activity to gate selective cations,
475 significant calcium influx was not observed, suggesting that MS-channels concerned in the
476 activation pathway allow entry of cations other than calcium ions and/or gate an
477 undetectable level of calcium ions that is not sufficient to activate calmodulin-NOS

signaling directly but is enough to depolarize the cell membrane.

Considering the possible implication of MS-channels in the mechano-sensing mechanism of satellite cell activation, it is worth noting the valuable study by Formigli et al. (25), which provided the first experimental evidence that the transient receptor potential canonical channel 1 (TRPC1) represents an essential component of stretch-activated cation channel signaling in the mouse C2C12 myoblast cell line, as assayed by whole-cell patch-clamp and atomic force microscopic pulling. That study indicated that TRPC1 plays a crucial role in mechano-transduction during regulation of the early phases of myoblast differentiation. TRPCs (TRPC1-7) are a family of cation channels that assemble as homo- or hetero-tetramers to form voltage-independent, non-selective cation- (Na^+ and Ca^{2+}) permeable pores (16, 46). Although numerous studies have shown that TRPC1 may be store-operated calcium-ion entry channels (SOCs) in various cell types (23, 74), there is also evidence that this channel is able to translate membrane stretch into cation currents across the plasma membrane (17, 37, 52). TRPC5 and 6 were also shown to be stretch-gated and GsMTx-4-sensitive cation-channels and TRPC6 plays an essential role of mehano-sensing in smooth muscle cells (26, 51; reviewed in Ref. 13), therefore, at least at this time, TRPC1, 5, and 6 may be reasonable candidates for the MS-channel in the satellite cell activation pathway concerned here. Our rat satellite cell cultures expressed TRPC1 message, as revealed by RT-PCR, while TRPC6 was not detected at 24-hr post-plating (Fig. 3 panel *B*), which is the time-point at which the stretch treatment was applied in the present and our previous experiments (65, 75-77); this provides a supportive background for the implication of TRPC1 in the above model of stretch-activation. TRPA1 (18), TRPV4 (10) and TRPM7 (41) are also reported to be stretch-sensitive channels and therefore can not be excluded from the list of candidate MS-channels at the present time, and the field awaits a study to examine their GsMTx-4 sensitivity and expression in quiescent satellite cells.

Another important observation by Formigli et al. (25) is that TRPC1 activity and stretch-induced cation influx in C2C12 myoblasts were modulated by sphingosine-1-phosphate (S1P), an important bioactive sphingolipid-metabolite that mainly acts through G-protein-coupled receptors present on mammalian cells, and thereby regulates numerous cell functions including cell proliferation, differentiation and apoptosis (78). In line with this, TRPC1 expression is reported to be significantly up-regulated during myogenesis, especially in the presence of S1P, supporting the physiological relevance of the sphingosine-S1P-TRPC1 axis in regulating C2C12 cell growth and differentiation (24, 25,

39). Notably, Nagata et al. (40) clearly showed that S1P can induce satellite cells to enter the cell cycle, whereas inhibiting the sphingolipid signaling cascade (which generates S1P mainly from sphingomyelin and sphingosine by N-SMase, ceramidase and sphingosine kinase) reduces the number of satellite cells able to divide in response to mitogen stimulation. A similar observation was reported by Sassoli et al. (48); S1P promotes satellite cell renewal and differentiation in damaged muscle. Although the S1P-mediated activation pathway is not well elucidated at the present time, considering the regulative role of S1P in TRPC1 gating in C2C12 myoblasts (25), one possible hypothesis may be that S1P associates with TRPC1 (and/or TRPC5, 6) directly or indirectly and can trigger satellite cell activation even without stretch stimuli. Alternatively, SIP could drastically decrease the threshold intensity of stretch that is required for TRPC gating; this would be followed by L-VGC-channel activation and lead to influx of extracellular calcium ions and their subsequent presentation to calmodulin to form calcium-calmodulin complexes as the cNOS activator. In line with this, it is worth noting the excellent study by Sbrana et al. (49), which showed that S1P activates the cytoskeleton contraction that in turn stretches the cell membrane and increases its stiffness; therefore such changes may improve the mechano-sensitivity of un-stretched C2C12 myoblasts. This S1P-TRPC scenario was recently addressed by some focused studies on TRPC functions related to sphingolipid biology, and therefore does not exclude other possibilities including that the S1P pathway is not dependent on either TRPC signaling or the activation cascade concerned here.

In summary, the present experiments bridge the gap between mechanical stretch stimuli and the increase in intracellular calcium-ion concentration by demonstrating that inhibition of MS-channels and L-VGC-channels in vitro, prior to mechanical stretch, prevents the influx of extracellular calcium ions, HGF-release from the matrix and re-entry of adult satellite cells into the cell cycle. The physiological significance of the MS-channel gating-initiated pathway described using cultured satellite cells remains to be verified in muscle fibers, as does the crucial role of calcium-calmodulin formation in the NO-radical production by cNOS that was described recently in isolated satellite cells in culture (67). Nonetheless, the current report demonstrated that in isolated satellite cells, a functional coupling of MS-channel and L-VGC-channel gating plays the central role in mechano-sensing machinery that instigates the activation of satellite cells.

ACKNOWLEDGMENTS

We are grateful to T. Tamura of Nikon Instech for technical assistance with the calcium imaging. The G3G4 mouse anti-BrdU monoclonal antibody developed by S. J. Kaufman and D3 anti-desmin monoclonal antibody developed by D. A. Fischman were obtained from the Developmental Studies Hybridoma Bank, developed under the auspices of the NICHD and maintained by The University of Iowa, Department of Biological Sciences, Iowa City, IA 52242, Iowa.

GRANTS

This work was supported by Grants-in-Aid for Scientific Research (B) 19380152 and 22380145 from the Japan Society for the Promotion of Science (JSPS) (all to R. Tatsumi) and by a research grant of the Graduate School Student Projects Academic Challenge 2010 from the Entrepreneurship Center of Kyushu University (to M. Hara). The research was also supported by funds from the Arizona Agriculture Experiment Station and grants from the US Department of Agriculture National Research Initiative Competitive Grant 2005-35206-15255 and Muscular Dystrophy Association Grant MDA3685 (all to R. E. Allen), and by funds from the Canadian Space Agency 9F007-52237-001-SR and the Natural Sciences and Engineering Research Council 171302 (to J. E. Anderson). M.-K. Q. Do received a scholarship from the Ministry of Education, Culture, Sports, Science and Technology-Japan (MEXT) during the course of this research.

REFERENCES

1. **Allen RE, Sheehan SM, Tayler RG, Kendall TL, Rice GM.** Hepatocyte growth factor activates quiescent skeletal muscle satellite cells in vitro. *J Cell Physiol* 165: 307–312, 1995.
2. **Allen RE, Temm-Grove CJ, Sheehan SM, Rice GM.** Skeletal muscle satellite cell cultures. *Methods Cell Biol* 52: 155-176, 1997.
3. **Andersen OS, Koeppe II RE.** Bilayer thickness and membrane protein function: an energetic perspective. *Annu Rev Biophys Biomol Struct* 36: 107-130, 2007.
4. **Anderson JE.** A role for nitric oxide in muscle repair: nitric oxide-mediated activation of muscle satellite cells. *Mol Biol Cell* 11: 1859-1874, 2000.
5. **Anderson JE, Pilipowicz O.** Activation of muscle satellite cells in single-fiber cultures. *Nitric Oxide* 7: 36-41, 2002.
6. **Anderson JE, Vargas C.** Correlated NOS-Imμ and myf5 expression by satellite cells in mdx mouse muscle regeneration during NOS manipulation and deflazacort treatment. *Neuromuscul Disord* 13: 388-396, 2003.
7. **Anderson JE, Wozniak AC.** Satellite cell activation on fibers: modeling events in vivo. *Can J Physiol Pharmacol* 82: 300-310, 2004.
8. **Anderson JE.** The satellite cell as a companion in skeletal muscle plasticity: currency, conveyance, clue, connector and colander. *J Exp Biol* 209: 2276-2292, 2006.
9. **Árnadóttir J, Chalfie M.** Eukaryotic mechanosensitive channels. *Annu Rev Biophys* 39: 111-137, 2010.
10. **Becker D, Blase C, Bereiter-Hahn J, Jendrach M.** TRPV4 exhibits a functional role in cell-volume regulation. *J Cell Sci* 118: 2435-2440, 2005.
11. **Bischoff R.** A satellite cell mitogen from crushed adult muscle. *Dev Biol* 115: 140-147, 1986.
12. **Bischoff R.** The satellite cell and muscle regeneration. In: *Myology*: Basic and Clinical, 2nd ed., edited by Engel AG and Franzini-Armstrong C. New York: McGraw-Hill, 1994, vol. 1, p. 97-118.
13. **Bowman CL, Gottlieb PA, Suchyna TM, Murphy YK, Sachs F.** Mechanosensitive ion channels and the peptide inhibitor GsMTx-4: history, properties, mechanisms and pharmacology. *Toxicon* 49: 249-270, 2007.
14. **Catterall WA.** Signaling complexes of voltage-gated sodium and calcium channels. *Neurosci Lett* 486: 107-116, 2010.
15. **Chargé SB, Rudnicki MA.** Cellular and molecular regulation of muscle regeneration. *Physiol Rev* 84: 209-238, 2004.
16. **Clapham DE.** TRP channels as cellular sensors. *Nature* 426: 517-524, 2003.
17. **Clark K, Middelbeek J, van Leeuwen FN.** Interplay between TRP channels and the cytoskeleton in health and disease. *Eur J Cell Biol* 87: 631-640, 2008.
18. **Corey DP, García-Añoveros J, Holt JR, Kwan KY, Lin SY, Vollrath MA, Amalfitano A, Cheung EL, Derfler BH, Duggan A, Géléoc GS, Gray PA, Hoffman MP, Rehm HL, Tamasauskas D, Zhang DS.** TRPA1 is a candidate for the mechanosensitive transduction channel of vertebrate hair cells. *Nature* 432: 723-730, 2004.
19. **Cornelison DDW, Wold BJ.** Single-cell analysis of regulatory gene expression in quiescent and activated mouse skeletal muscle satellite cells. *Dev Biol* 191: 270-283, 1997.

20. **Derksen PW, Keehnen RM, Evers LM, van Oers MH, Spaargaren M, Pals ST.** Cell surface proteoglycan syndecan-1 mediates hepatocyte growth factor binding and promotes Met signaling in multiple myeloma. *Blood* 99: 1405-1410, 2002.
21. **Dulhunty AF.** Excitation-contraction coupling from the 1950s into the new millennium. *Clin Exp Pharmacol Physiol* 33: 763-772, 2006.
22. **Engelman DM.** Membranes are more mosaic than fluid. *Nature* 438: 578-580, 2005.
23. **Fiorio Pla A, Maric D, Brazer SC, Giacobini P, Liu X, Chang YM, Ambudkar IS, Barker JL.** Canonical transient receptor potential 1 plays a role in basic fibroblast growth factor (bFGF)/FGF receptor-1-induced Ca^{2+} entry and embryonic rat neural stem cell proliferation. *J Neurosci* 25: 2687-2701, 2005.
24. **Formigli L, Meacci E, Sassoli C, Squecco R, Nosi D, Chellini F, Naro F, Francini F, Zecchi-Orlandini S.** Cytoskeleton/stretch-activated ion channel interaction regulates myogenic differentiation of skeletal myoblasts. *J Cell Physiol* 211: 296-306, 2007.
25. **Formigli L, Sassoli C, Squecco R, Bini F, Martinesi M, Chellini F, Luciani G, Sbrana F, Zecchi-Orlandini S, Francini F, Meacci E.** Regulation of transient receptor potential canonical channel 1 (TRPC1) by sphingosine 1-phosphate in C2C12 myoblasts and its relevance for a role of mechanotransduction in skeletal muscle differentiation. *J Cell Sci* 122: 1322-1333, 2009.
26. **Gomis A, Soriano S, Belmonte C, Viana, F′.** Hypoosmotic- and pressure-induced membrane stretch activate TRPC5 channels. *J Physiol* 586: 5633-5649, 2008.
27. **Haswell ES, Phillips R, Rees DC.** Mechanosensitive channels: what can they do and how do they do it? *Structure* 19: 1356-1369, 2011.
28. **Hawke TJ, Garry DJ.** Myogenic satellite cells: physiology to molecular biology. *J Appl Physiol* 91: 534-551, 2001.
29. **Huang L, Keyser BM, Tagmose TM, Hansen JB, Taylor JT, Zhuang H, Zhang M, Ragsdale DS, Li M.** NNC 55-0396 [(1S,2S)-2-(2-(N-[(3-benzimidazol-2-yl)propyl]-N-methylamino)ethyl)-6-fluoro-1,2,3, 4-tetrahydro-1-isopropyl-2-naphtyl cyclopropanecarboxylate dihydrochloride]: a new selective inhibitor of T-type calcium channels. *J Pharmacol Exp Ther* 309: 193-199, 2004.
30. **Johnson SE, Allen RE.** Proliferating cell nuclear antigen (PCNA) is expressed in activated rat skeletal muscle satellite cells. *J Cell Physiol* 154: 39-43, 1993.
31. **Kobayashi T, Sokabe M.** Sensing substrate rigidity by mechanosensitive ion channels with stress fibers and focal adhesions. *Curr Opin Cell Biol* 22: 669-676, 2010.
32. **Kuang S, Gillespie MA, Rudnicki MA.** Niche regulation of muscle satellite cell self-renewal and differentiation. *Cell Stem Cell* 2: 22-31, 2008.
33. **Kung C, Martinac B, Sukharev S.** Mechanosensitive channels in microbes. *Annu Rev Microbiol* 64: 313-329, 2010.
34. **Lacinová L.** Voltage-dependent calcium channels. *Gen Physiol Biophys* 24: 1-78, 2005.
35. **Laemmli UK.** Cleavage of structural proteins during the assembly of the head of bacteriophage T4. *Nature* 277: 680-685, 1970.
36. **Lipscombe D, Helton TD, Xu W.** L-type calcium channels: the low down. *J Neurophysiol* 92: 2633-2641, 2004.

37. **Maroto R, Raso A, Wood TG, Kurosky A, Martinac B, Hamill OP.** TRPC1 forms the stretch-activated cation channel in vertebrate cells. *Nature Cell Biol* 7: 179-185, 2005.
38. **Martins KJB, Maclean I, Murdoch GK, Dixon WT, Putman CT.** Nitric oxide synthase inhibition delays low frequency stimulation-induced satellite cell activation in rat fast-twitch muscle. *Appl Physiol Nutr Metab* 36: 996-1000, 2011.
39. **Meacci E, Nuti F, Donati C, Cencetti F, Farnararo M, Bruni P.** Sphingosine kinase activity is required for myogenic differentiation of C2C12 myoblasts. *J Cell Physiol* 214: 210-220, 2008.
40. **Nagata Y, Partridge TA, Matsuda R, Zammit PS.** Entry of muscle satellite cells into the cell cycle requires sphingolipid signaling. *J Cell Biol* 174: 245-253, 2006.
41. **Numata T, Shimizu T, Okada Y.** TRPM7 is a stretch- and swelling-activated cation channel involved in volume regulation in human epithelial cells. *Am J Physiol Cell Physiol* 292: C460-C467, 2007.
42. **Perozo E, Cortes DM, Sompornpisut P, Kloda A, Martinac B.** Open channel structure of MscL and the gating mechanism of mechanosensitive channels. *Nature* 418: 942-948, 2002.
43. **Persechini A, McMillan K, Leakey P.** Activation of myosin light chain kinase and nitric oxide synthase activities by calmodulin fragments. *J Biol Chem* 269: 16148-16154, 1994.
44. **Rios E, Brum G.** Involvement of dihydropyridine receptors in excitation-contraction coupling in skeletal muscle. *Nature* 325: 717-720, 1987.
45. **Roel W ten Broek, Grefte S, Johannes W Von den Hoff.** Regulatory factors and cell populations involved in skeletal muscle regeneration. *J Cell Physiol* 224: 7-16, 2010.
46. **Rychkov G, Barritt GJ.** TRPC1 Ca^{2+}-permeable channels in animal cells. *Handb Exp Pharmacol* 179: 23-52, 2007.
47. **Sakata T, Tatsumi R, Yamada M, Shiratsuchi S, Okamoto S, Mizunoya W, Hattori A, Ikeuchi Y.** Preliminary experiments on mechanical stretch-induced activation of skeletal muscle satellite cells in vivo. *Anim Sci J* 77: 518-525, 2006.
48. **Sassoli C, Formigli L, Bini F, Tani A, Squecco R, Battistini C, Zecchi-Orlandini S, Francini F, Meacci E.** Effects of S1P on skeletal muscle repair/regeneration during eccentric contraction. *J Cell Mol Med* 15: 2498-2511, 2011.
49. **Sbrana F, Sassoli C, Meacci E, Nosi D, Squecco R, Paternostro F, Tiribilli B, Zecchi-Orlandini S, Francini F, Formigli L.** Role for stress fiber contraction in surface tension development and stretch-activated channel regulation in C2C12 myoblasts. *Am J Physiol Cell Physiol* 295: C160-C172, 2008.
50. **Seale P, Rudnicki MA.** A new look at the origin, function, and "Stem-Cell" status of muscle satellite cells. *Dev Biol* 218: 115-124, 2000.
51. **Spassova MA, Hewavitharana T, Xu W, Soboloff J, Gill DL.** A common mechanism underlies stretch activation and receptor activation of TRPC6 channels. *Proc Natl Acad Sci USA* 103: 16586-16591, 2006.
52. **Stiber JA, Zhang ZS, Burch J, Eu JP, Zhang S, Truskey GA, Seth M, Yamaguchi N, Meissner G, Shah R, Worley PF, Williams RS, Rosenberg PB.** Mice lacking Homer 1 exhibit a skeletal myopathy characterized by abnormal transient receptor potential channel activity. *Mol Cell Biol* 28: 2637-2647, 2008.

53. **Striessnig J.** Ca^{2+} channel blockers. In: *Encyclopedic reference of molecular pharmacology*, edited by Offermanns S and Rosenthal W. Berlin: Springer, 2004, p. 201-207.

54. **Suchyna TM, Tape SE, Koeppe RE II, Andersen OS, Sachs F, Gottlieb PA.** Bilayer-dependent inhibition of mechanosensitive channels by neuroactive peptide enantiomers. *Nature* 430: 235-240, 2004.

55. **Tai CH, Yang YC, Pan MK, Huang CS, Kuo CC.** Modulation of subthalamic T-type Ca^{2+} channels remedies locomotor deficits in a rat model of Parkinson disease. *J Clin Invest* 121: 3289-3305, 2011.

56. **Takenaka T, Suzuki H, Okada H, Hayashi K, Ozawa Y, Saruta T.** Biophysical signals underlying myogenic responses in rat interlobular artery. *Hypertension* 32: 1060-1065, 1998a.

57. **Takenaka T, Suzuki H, Okada H, Hayashi K, Kanno Y, Saruta T.** Mechanosensitive cation channels mediate afferent arteriolar myogenic constriction in the isolated rat kidney. *J Physiol* 511: 245-253, 1998b.

58. **Tatsumi R, Anderson JE, Nevoret CJ, Halevy O, Allen RE.** HGF/SF is present in normal adult skeletal muscle and is capable of activating satellite cells. *Dev Biol* 194: 114-128, 1998.

59. **Tatsumi R, Sheehan SM, Iwasaki H, Hattori A, Allen RE.** Mechanical stretch induces activation of skeletal muscle satellite cells in vitro. *Exp Cell Res* 267: 107-114, 2001.

60. **Tatsumi R, Hattori A, Ikeuchi Y, Anderson JE, Allen RE.** Release of hepatocyte growth factor from mechanically stretched skeletal muscle satellite cells and role of pH and nitric oxide. *Mol Biol Cell* 13: 2909-2918, 2002a.

61. **Tatsumi R, Hattori A, Allen RE, Ikeuchi Y, Ito T.** Mechanical stretch-induced activation of skeletal muscle satellite cells is dependent on nitric oxide production in vitro. *Anim Sci J* 73: 235-239, 2002b.

62. **Tatsumi R, Allen RE.** Active hepatocyte growth factor is present in skeletal muscle extracellular matrix. *Muscle Nerve* 30: 654-658, 2004.

63. **Tatsumi R, Mitsuhashi K, Ashida K, Haruno A, Hattori A, Ikeuchi Y, Allen RE.** Comparative analysis of mechanical stretch-induced activation activity of back and leg muscle satellite cells in vitro. *Anim Sci J* 75: 345-351, 2004.

64. **Tatsumi R, Liu X, Pulido A, Morales M, Sakata T, Dail S, Hattori A, Ikeuchi Y, Allen RE.** Satellite cell activation in stretched skeletal muscle and the role of nitric oxide and hepatocyte growth factor. *Am J Physiol Cell Physiol* 290: C1487-C1494, 2006a.

65. **Tatsumi R, Yamada M, Katsuki Y, Okamoto S, Ishizaki J, Mizunoya W, Ikeuchi Y, Hattori A, Shimokawa H, Allen RE.** Low-pH preparation of skeletal muscle satellite cells can be used to study activation in vitro. *Int J Biochem Cell Biol* 38: 1678-1685, 2006b.

66. **Tatsumi R, Allen RE.** Mechano-biology of resident myogenic stem cells: molecular mechanism of stretch-induced activation of satellite cells. *Anim Sci J* 79: 279-290, 2008.

67. **Tatsumi R, Wuollet AL, Tabata K, Nishimura S, Tabata S, Mizunoya W, Ikeuchi Y, Allen RE.** A role for calcium-calmodulin in regulating nitric oxide production during skeletal muscle satellite cell activation. *Am J Physiol Cell Physiol* 296: C922-C929, 2009.

68. **Tatsumi R.** Mechano-biology of skeletal muscle hypertrophy and regeneration: possible mechanism of stretch-induced activation of resident myogenic stem cells. *Anim Sci J* 81: 11-20, 2010.
69. **Weissman BA, Jones CL, Liu Q, Gross SS.** Activation and inactivation of neuronal nitric oxide synthase: characterization of Ca^{2+}-dependent [^{125}I]calmodulin binding. *Eur J Pharmacol* 435: 9-18, 2002.
70. **Welsh DG, Morielli AD, Nelson MT, Brayden JE.** Transient receptor potential channels regulate myogenic tone of resistance arteries. *Circ Res* 90: 248-250, 2002.
71. **Wozniak AC, Pilipowicz O, Yablonka-Reuveni Z, Greenway S, Craven S, Scott E, Anderson JE.** C-met expression and mechanical activation of satellite cells on cultured muscle fibers. *J Histochem Cytochem* 51: 1-9, 2003.
72. **Wozniak AC, Kong J, Bock E, Pilipowicz O, Anderson JE.** Signaling satellite-cell activation in skeletal muscle: markers, models, stretch, and potential alternate pathways. *Muscle Nerve* 31: 283-300, 2005.
73. **Wozniak AC, Anderson JE.** Nitric oxide-dependence of satellite stem cell activation and quiescence on normal skeletal muscle fibers. *Dev Dyn* 236: 240-250, 2007.
74. **Wu X, Zagranichnaya TK, Gurda GT, Eves EM, Villereal ML.** A TRPC1/TRPC3-mediated increase in store-operated calcium entry is required for differentiation of H19-7 hippocampal neuronal cells. *J Biol Chem* 279: 43392-43402, 2004.
75. **Yamada M, Tatsumi R, Kikuiri T, Okamoto S, Nonoshita S, Mizunoya W, Ikeuchi Y, Shimokawa H, Sunagawa K, Allen RE.** Matrix metalloproteinases are involved in mechanical stretch-induced activation of skeletal muscle satellite cells. *Muscle Nerve* 34: 313-319, 2006.
76. **Yamada M, Sankoda Y, Tatsumi R, Mizunoya W, Ikeuchi Y, Sunagawa K, Allen RE.** Matrix metalloproteinase-2 mediates stretch-induced activation of skeletal muscle satellite cells in a nitric oxide dependent manner. *Int J Biochem Cell Biol* 40: 2183-2191, 2008.
77. **Yamada M, Tatsumi R, Yamanouchi K, Hosoyama T, Shiratsuchi S, Sato A, Ikeuchi Y, Furuse M, Allen RE.** High concentrations of HGF inhibit skeletal muscle satellite cell proliferation in vitro by inducing expression of myostatin: a possible mechanism for reestablishing satellite cell quiescence in vivo. *Am J Physiol Cell Physiol* 298: C465-C476, 2010.
78. **Zeidan YH, Hannun YA.** Translational aspects of sphingolipid metabolism. *Trends Mol Med* 13: 327-336, 2007.

794 **FIGURE LEGENDS**

795 Fig. 1. Significance of extracellular calcium ions in stretch-activation of satellite cells in
796 vitro. Satellite cells from adult rat skeletal muscle were stretched in culture (*black bars*)
797 for 1 hr beginning at 24-hr post-plating in FlexerCell FX-2000 System (25% stretch at
798 12-sec intervals, as originally optimized in Tatsumi et al. (59) and shown in panel *A* again)
799 in the presence (*bar d*) or absence (*bar c*) of 1.8 mM ethyleneglycol tetraacetic acid (EGTA)
800 in DMEM-10% normal horse serum (pH 7.2), followed an assay to detect activation using
801 bromodeoxyuridine (BrdU) at 48-hr post-plating. This experiment also included the
802 following control cultures: *bar a*, un-stretched culture; *bar b*, 2-hr stretch culture
803 (equivalent to our regular period of stretch, originally described in Ref. 59); *bar e*, stretched
804 culture receiving 1.8 mM EGTA for 24-48 hr post-plating; *bar f*, positive control culture
805 supplemented with 2.5 ng/ml recombinant mouse hepatocyte growth factor (HGF) for 24-48
806 hr; *bar g*, HGF culture receiving 1.8 mM EGTA for 24-48 hr; *bars h* and *i*, control cultures
807 with 1.8 mM EGTA for 24-25 hr and 24-48 hr, respectively. Bars depict mean and
808 standard error for four cultures per treatment; double asterisks indicate that the treatment
809 mean was significantly different from the mean of positive control cultures (*bar f*) at $p <$
810 0.01. *NS*, no significant difference ($p > 0.05$) in the activation index.
811
812 Fig. 2. Dose-dependent effect of cation-channel inhibitors on stretch-activation of satellite
813 cells and up-stream HGF release. Panel *A*, satellite cells were subjected to an environment
814 of cyclic stretch for 1 hr beginning at 24-hr post-plating in the presence of various
815 concentrations of individual cation-channel inhibitors, GsMTx-4 (*closed circle*), nifedipine
816 (*closed square*), gadolinium chloride (*open circle*), and NNC55-0396 (*open square*), and
817 assayed for BrdU-incorporation at 48-hr post-plating. This experiment also included
818 control cultures as follows: *bar a*, un-stretched culture (*white bar*); *bar b*, 1-hr stretch
819 culture (*black bar* marked *Positive Control*); bars c-g, control cultures receiving 2.5 ng/ml
820 HGF at 24-48 hr post-plating along with none, 0.1 μM GsMTx-4, 10 μM nifedipine, 100
821 μM gadolinium chloride, and 100 μM NNC55-0396, respectively (*grayed bars*); *bars h-j*,
822 un-stretched cultures with individual cation-channel inhibitors (each at the optimal
823 concentration). Data points and bars depict mean and standard error of four cultures per
824 treatment; single and double asterisks indicate that the treatment mean was significantly
825 different from the mean of positive control cultures (*bar b*) at $p < 0.05$ and $p < 0.01$,
826 respectively. Panel *B*, a typical data set of ECL-western blotting of HGF in two or three

827 independent experiments; conditioned media (serum-free DMEM) from 1-hr stretch
828 cultures with none (*lane m*), 0.1 μM GsMTx-4 (*lane n*), 10 μM nifedipine (*lane o*) or 1.8
829 mM EGTA (*lane p*), were analyzed for HGF release from the extracellular tethering by
830 ECL-western blotting standardized with internal β-actin in cell lysates that were harvested
831 after stretch. *Lane q*, un-stretch medium; *k*, molecular weight standards (STD); *l*, mouse
832 recombinant HGF (12 ng) to show the band at 60-kDa α-chain for active HGF (*upper row*)
833 and 42-kDa β-actin in mouse C2C12 myoblasts (*lower row*) as positive controls (PC); *r*,
834 negative controls (NC) of stretch medium (*upper row*) and whole cell lysate (*lower row*)
835 blotted without the primary antibody and with secondary antibody.
836
837 Fig. 3. Detection of mRNA for the L-type voltage-gated calcium channel
838 (L-VGC-channel) and transient receptor potential canonical channels 1 and 6 (TRPC1, 6) in
839 satellite cells. Satellite cell cultures were maintained in DMEM-10% HS and assayed for
840 mRNA expression of α_{1S}, α_{1C}, α_{1D}, α_{1F} subunits of the L-VGC-channel (panel *A*) and
841 TRPC1, 6 (panel *B*) at 24-hr post-plating by RT-PCR. Bands were visualized with
842 Gel-Red staining after agarose gel electrophoresis. *NC*, negative controls (satellite cell
843 mRNA without reverse transcription); *SCs*, satellite cells; *PC*, positive controls (rat skeletal
844 muscle for α_{1S} and TRPC1, cardiac muscle for α_{1C}, brain for α_{1D} and TRPC6, and eye for
845 α_{1F}).
846
847 Fig. 4. Effect of cation-channel inhibitors and EGTA on the increase in intracellular
848 calcium ion concentration in response to stretch. Calcium-imaging analysis was conducted
849 under the StageFlexer Jr. system using Fluo3-loaded satellite cells that were treated with
850 individual cation-channel inhibitors (0.1 μM GsMTx-4, 10 μM nifedipine) for 30-min just
851 prior to adding two cycles of stretch at 24-hr post-plating. Row *+EGTA*, cells were
852 incubated with 1.8 mM EGTA in DMEM-10% HS just prior to the addition of the stretch.
853 Companion cells were treated with 3 μM A23187 (a calcium ionophore) and served as a
854 positive control (row *A23187*) (67). Fluorescence intensity was assigned from blue to red
855 in color-coded images; the normal resting free calcium-ion level was represented by blue,
856 and gradual increases were demonstrated by a change to yellow and then red. After
857 calcium imaging, cells were visualized by immunostaining to confirm the presence of c-met,
858 a marker molecule for myogenic cells in our primary cell cultures (DAB-stained images not
859 shown).

Fig. 5. A possible mechanism of satellite cell activation in response to mechanical stimuli. Panel *A*, reproduced from Fig. 4 of Tatsumi and Allen (66) with some modifications. Ca-CaM, calcium-calmodulin complex; L-Arg, L-arginine; NOS, NO synthase; MMP2, matrix metalloproteinase 2. Panel *B*, calcium ion influx mechanism was examined in the present study and the model was schematically presented. Steps 1 and 2: cations stream into the cell through mechano-sensitive cation channels (MS-channel) to induce local depolarization of the cell membrane (changes in membrane potential); step 3: depolarization promotes gating of adjacent L-type voltage-gated calcium-ion channels (L-VGC-channel), and the result is calcium ion influx that promotes formation of the Ca-CaM complex that initiates NOS activity.

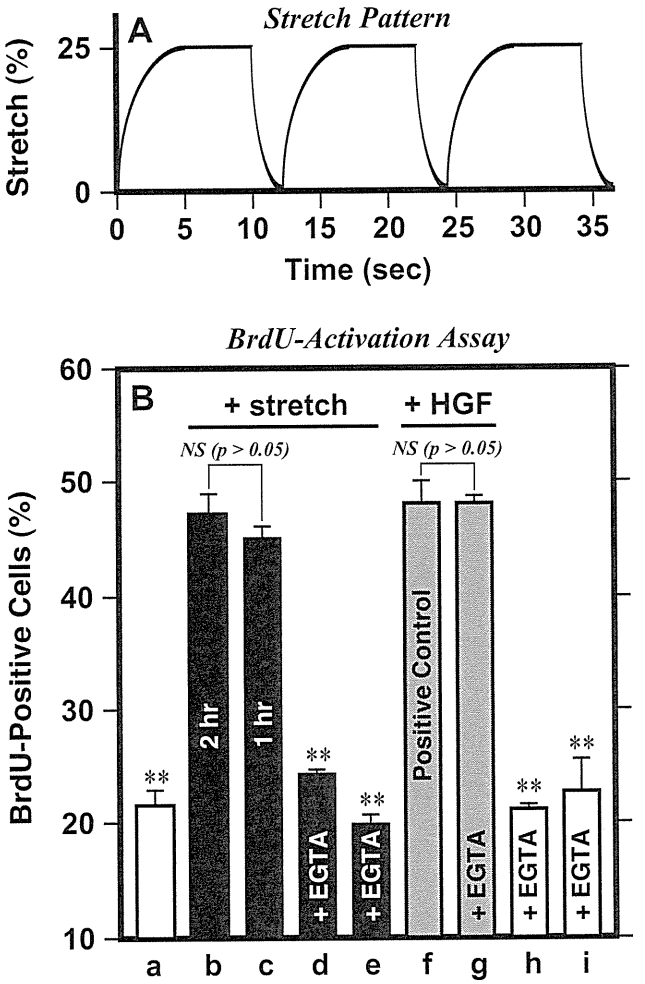

Fig. 1, Hara *et al.*

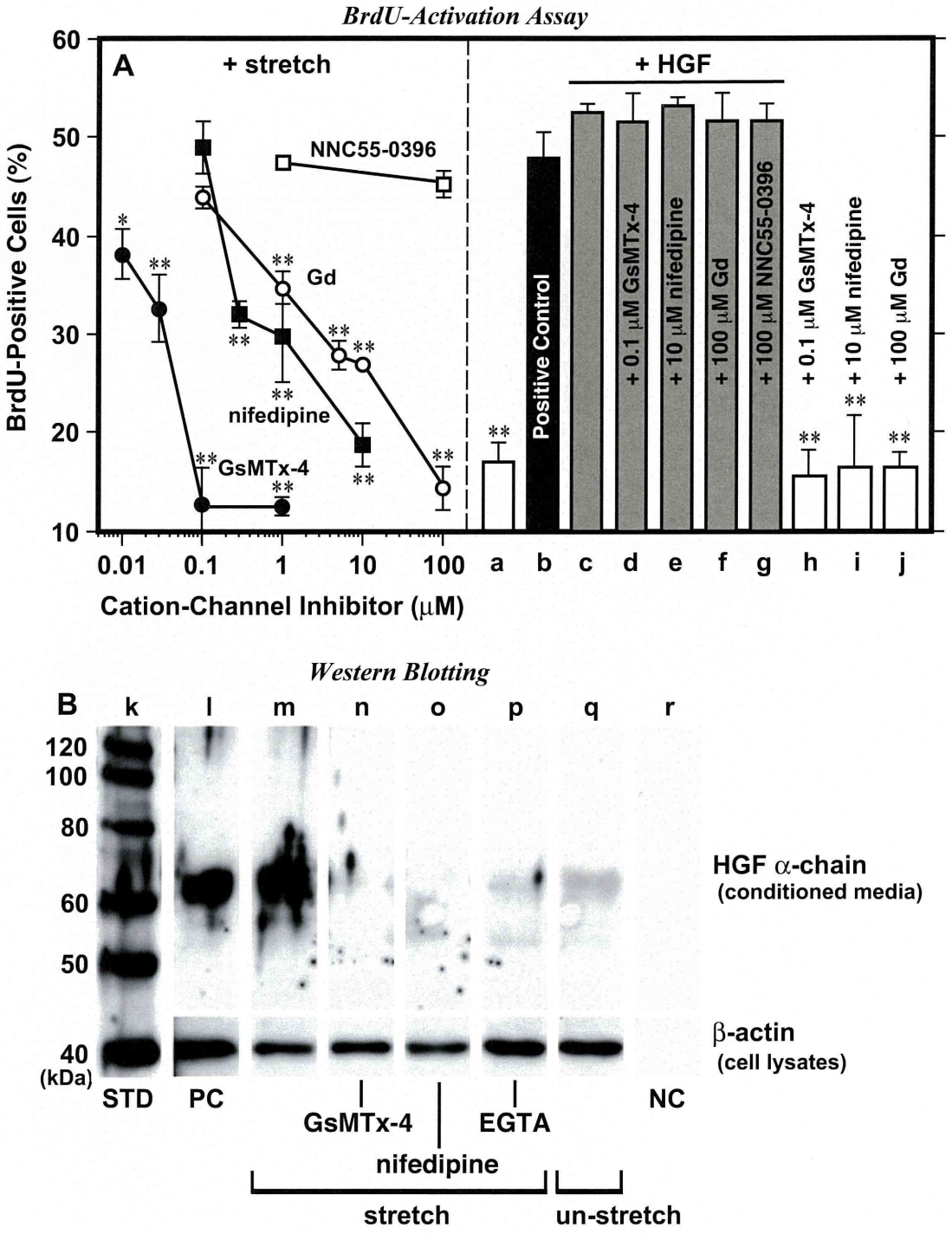

Fig. 2, Hara *et al.*

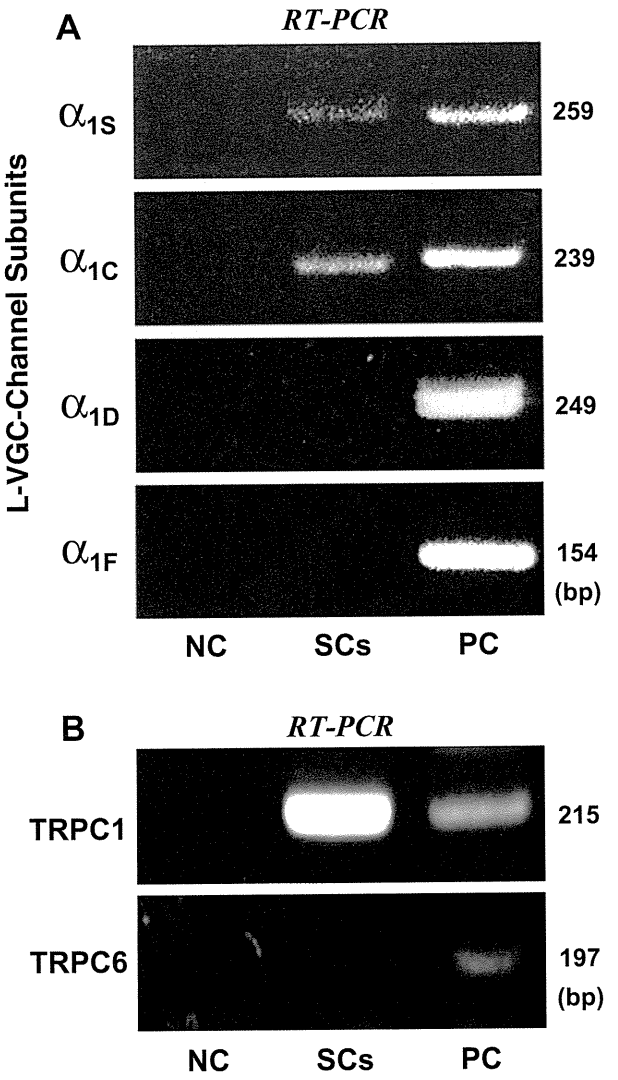

Fig. 3, Hara *et al.*

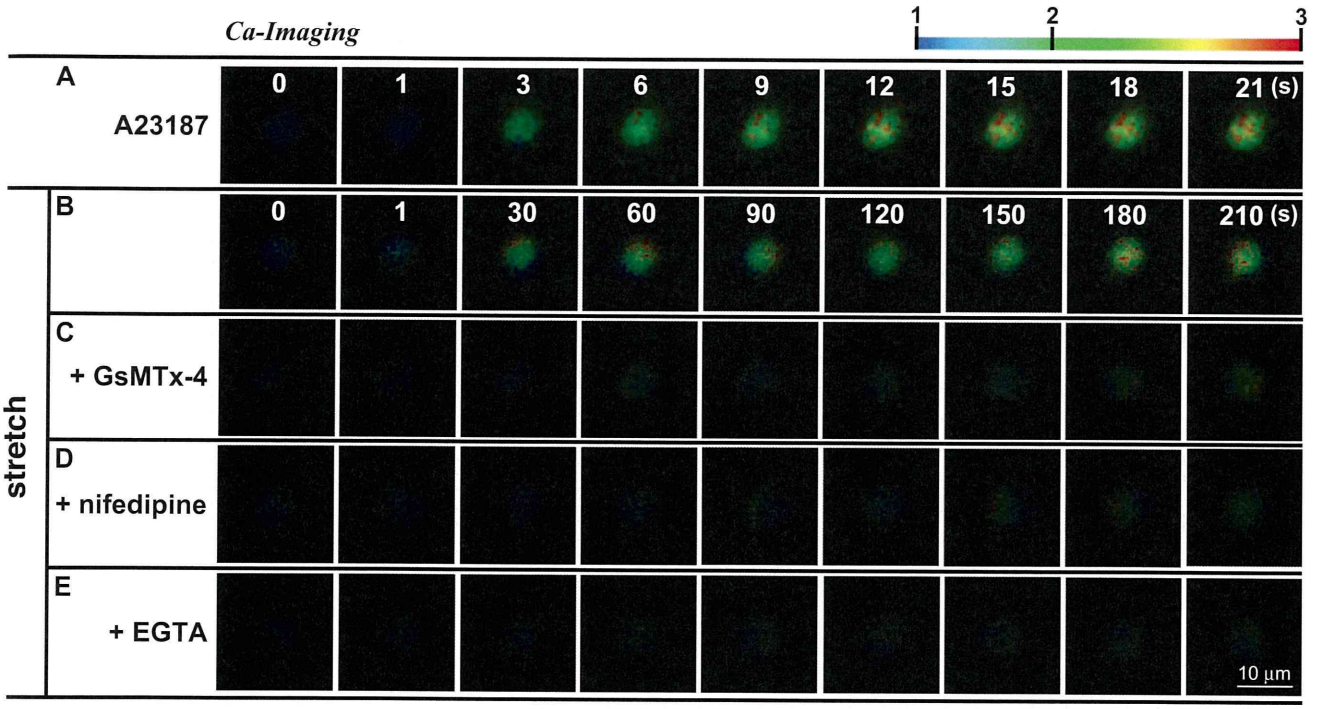

Fig. 4, Hara *et al.*

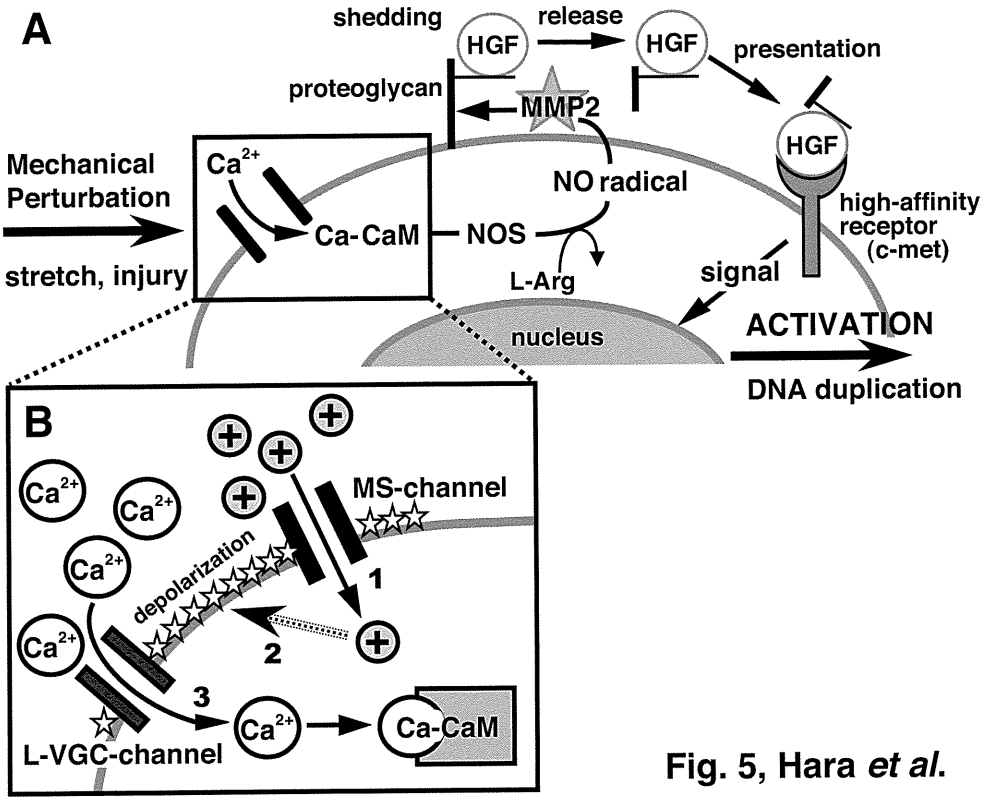

Fig. 5, Hara *et al.*

Beraprost sodium, a stable prostacyclin analogue, improves insulin resistance in high-fat diet-induced obese mice

Eriko Inoue[1], Toshihiro Ichiki[1,2], Kotaro Takeda[1,2], Hirohide Matsuura[1], Toru Hashimoto[1], Jiro Ikeda[1], Aya Kamiharaguchi[1] and Kenji Sunagawa[1]

Departments of [1]Cardiovascular Medicine and [2]Advanced Therapeutics for Cardiovascular Diseases, Kyushu University Graduate School of Medical Sciences, Fukuoka, Japan

(Correspondence should be addressed to T Ichiki at Department of Advanced Therapeutics for Cardiovascular Diseases, Kyushu University Graduate School of Medical Sciences; Email: ichiki@cardiol.med.kyushu-u.ac.jp)

Abstract

Obesity induces hypertrophy of adipocyte resulting in production of pro-inflammatory cytokines such as tumor necrosis factor-α (TNF-α) and monocyte chemoattractant protein 1 (MCP1 (CCL2)). These cytokines play an important role in the development of insulin resistance. Beraprost sodium (BPS), a prostaglandin I_2 analogue, is reported to attenuate inflammation. In this study, we examined the effect of BPS on glucose metabolism in mice fed a high-fat diet (HFD). Four-week-old C57/B6 male mice were fed a HFD for 12 weeks (HFD group) and the treatment group received oral BPS (300 μg/kg per day) for the same period. Then, glucose metabolism, histological changes, and gene expression of white adipose tissue (WAT) were examined. Body weight was increased, and glucose intolerance and insulin resistance were developed in the HFD group. Treatment with BPS improved glucose tolerance and insulin action without body weight change. Histological analysis of WAT showed an increase in the size of adipocyte and macrophage infiltration in the HFD group, which was attenuated by BPS treatment. BPS reduced HFD-induced expression of MCP1 and TNF-α in WAT. BPS also attenuated hepatic steatosis induced by the HFD. These results suggest that BPS improved glucose intolerance possibly through suppression of inflammatory cytokines in WAT. BPS may be beneficial for the treatment of obesity-associated glucose intolerance.

Journal of Endocrinology (2012) **213,** 285–291

Introduction

Obesity plays a central role in the development of metabolic syndrome (Wajchenberg 2000), a constellation of risk factors such as insulin resistance, dyslipidemia, and high blood pressure. Accumulation of visceral fat rather than subcutaneous fat is believed to cause insulin resistance (Wajchenberg 2000, Masuzaki *et al.* 2001). In obesity, adipocytes are enlarged and increased in number, and an excess of lipid leads to ectopic deposition of triglyceride in the liver and muscle, which is one of the causes of insulin resistance (Savage *et al.* 2007). The hypertrophied adipocytes produce proinflammatory cytokines such as monocyte chemoattractant protein-1 (MCP1 (CCL2)) and tumor necrosis factor-α (TNF-α) as obesity progresses (Shoelson *et al.* 2006). These cytokines, so-called adipokines, cause inflammation and recruitment of macrophages to adipose tissue (Xu *et al.* 2003), which is another important mechanism for obesity-induced insulin resistance. The infiltrated macrophages enhance inflammation of adipose tissue, indicating that these processes form a vicious circle.

TNF-α induces c-Jun amino-terminal kinase (JNK) activation and phosphorylation of insulin receptor substrate 1 (IRS1) at serine residues that negatively regulate normal signaling through the insulin receptor/IRS1 axis (Hotamisligil *et al.* 1996). Mice lacking chemokine receptor-2 (CCR2), a receptor for MCP1, are partly protected against developing high-fat diet (HFD)-induced insulin resistance and exhibit reductions in adipose tissue macrophage recruitment and inflammatory gene expression (Weisberg *et al.* 2006). These observations suggest that adipose tissue in obesity is characterized by chronic low-grade inflammation, and inflammatory cytokines play a causative role in the development of insulin resistance.

Beraprost sodium (BPS) is a stable prostaglandin I_2 analogue and has a potent vasodilating effect through activation of prostacyclin receptor (Olschewski *et al.* 2004). BPS is also reported to attenuate inflammation. BPS reduced serum TNF-α levels in diabetic patients (Fujiwara *et al.* 2004) and expression of *Mcp1* mRNA in the kidney of Otsuka Long-Evans Tokushima fatty (OLETF) rats, resulting in the amelioration of diabetic nephropathy (Watanabe *et al.* 2009). BPS inhibits

0022–0795/12/0213–285 *Printed in Great Britain*

DOI: 10.1530/JOE-12-0014
Online version via http://www.endocrinology-journals.org

TNF-α-induced expression of vascular cell adhesion molecule and monocyte attachment to endothelial cells (Goya *et al.* 2003). We therefore hypothesized that the anti-inflammatory effects of BPS may be beneficial for the improvement of obesity-induced insulin resistance, in which inflammation plays an important role.

We showed in this study that BPS improved glucose metabolism in association with reduction of inflammation of white adipose tissue (WAT) in a mouse model of diet-induced obesity.

Materials and Methods

Animals

All procedures were approved by the institutional animal use and care committee and were conducted in conformity with institutional guidelines. Four-week-old C57/B6 mice were purchased from Kyudo Co. Ltd. (Tosu, Saga, Japan). Three groups were analyzed: mice fed a normal chow diet (control group), mice fed a HFD containing 60% kcal fat (High Fat Diet 32, Clea Japan (Tokyo); HFD group) for 12 weeks, and mice fed a HFD and administered BPS for 12 weeks (BPS group). BPS dissolved in water at 1·5 μg/ml was given *ad libitum* because of the short half-life of BPS (~1 h). As a preliminary study showed that the estimated volume of water intake was ~0·2 ml/g per day, the estimated dose of orally ingested BPS was 300 μg/kg per day. At the end of the experiment, systolic blood pressure (SBP) and heart rate (HR) were measured by a tail-cuff method (BP-98A, Softron Co., Tokyo, Japan). Mice were killed by CO_2 inhalation.

Histological analysis

Adipose tissues were fixed with 10% formaldehyde for 24 h. The specimens were embedded into paraffin. Paraffin sections were stained with hematoxylin and eosin (H&E). The cross-sectional area for each adipocyte was determined using Dynamic cell count BZ-HIC (Keyence, Osaka, Japan). To detect macrophage infiltration, the paraffin sections were stained with an antimouse MAC3 (LAMP2) antibody (Santa Cruz Biotechnology, Inc., Santa Cruz, CA, USA). Sections were deparaffinized with xylene and refixed with ethanol for 40 min, immersed in PBS, and then autoclaved in citrate buffer for antigen retrieval. Then, the sections were incubated with 3% hydrogen peroxide in methanol for 20 min. The sections were further incubated with an antibody against MAC3 (1:200) overnight at 4 °C. After rinsing with PBS, the sections were incubated with biotin-labeled goat anti-rabbit IgG antiserum (Santa Cruz Biotechnology, Inc., 1:200 dilution) for 30 min and then incubated with avidin–biotin complex (Vectastain ABC kit; 1:100 dilution) for 15 min, and the sections were incubated with 3,3-diaminobenzidine and 0·03% hydrogen peroxide in deionized water for about 80 s. The number of MAC3-positive cell clusters was counted in high power field (HPF). The data are mean of five randomly chosen HPFs. After the mice were killed, the livers were removed and subsequently fixed in 10% formaldehyde. The sections were embedded in paraffin blocks and stained with H&E to examine the structures of the liver and evaluate lipid droplets. For the quantification of areas of lipid accumulation in the liver, H&E-stained images of liver were uploaded into a computer for analysis. The images were processed into two gradations (black and white). The white porosity areas were quantified as vacuolation (Sato *et al.* 2010), which mostly represents accumulation of lipid droplets. Contribution of arteries, veins, and bile ducts to porosity area was small and equally observed in the three groups and therefore ignored in the quantification. The data are expressed as a percentage of white area to total area.

Glucose tolerance test and insulin tolerance test

Mice were starved for 6 h. Then, the mice were i.p. injected with glucose (1 g/kg of body weight) for the glucose tolerance test (GTT). For the insulin tolerance test (ITT), the mice were i.p. injected with rapid insulin (0·5 IU/kg of body weight). Blood was taken from tail vein at various time points to measure blood glucose concentrations by Glutest Every (Sanwa Kagaku Kenkyusho, Nagoya, Japan).

Measurement of serum levels of triglyceride, cholesterol, and insulin

Serum triglyceride and total cholesterol levels were determined by commercially available kits, Triglyceride E-test Wako (Wako, Osaka, Japan) and Cholesterol E-test Wako (Wako) respectively. Serum insulin levels were determined by ELISA kit (Morinaga Institute of Biological Science, Yokohama, Japan).

RNA extraction and real-time quantitative RT-PCR analysis

RNA from adipose tissue was extracted using ISOGEN according to the manufacturer's instruction (Wako). One microgram of total RNA was reverse transcribed using ReverTra Ace qPCR RT Kit (Toyobo, Osaka, Japan). Real-time quantitative PCR (qPCR) was performed using 7500 real-time PCR system (Applied Biosystems) and SYBER Green PCR Master Mix (Applied Biosystems). Primer sequences for real-time qPCR used in this study are as follows:

TNF-α: 5′-AAGCCTGTAGCCCACGTCGTA-3′;
5′-GGCACCACTAGTTGGTTGTCTTTG-3′.
MCP1: 5′-TTAACGCCCCCACTCACCTGCTG-3′;
5′-GCTTCTTTGGGACACCTGCTGC-3′.
PPARγ (PPARG):
5′-TGTCGGTTTCAGAAGTGCCTTG-3′;
5′-TTCAGCTGGTCGATATCACTGGAG-3′.
C/EBPα: 5′-TTGAAGCACAATCGATCCATCC-3′;
5′-GCACACTGCCATTGCACAAG-3′.
Adiponectin: 5′-GTCAGTGGATCTGACGACACCAA-3′;
5′-ATGCCTGCCATCCAACCTG-3′.
18S rRNA: 5′-ACTCAACACGGGAAACCTCA-3′;
5′-AACCAGACAAATCGCTCCAC-3′.

The expression of each gene was normalized with that of *18s* rRNA.

ELISA

ELISA for adiponectin and TNF-α was performed using commercially available kits (R&D systems, Inc., Minneapolis, MN, USA) in accordance with the manufacturer's instructions.

Statistical analysis

Statistical analysis was performed with one-way ANOVA and Fisher's test if appropriate. Data are shown as mean±S.E.M. $P<0{\cdot}05$ was considered to be statistically significant.

Results

Hemodynamic and metabolic parameters

Body weight was significantly increased in the HFD group compared with the control group at the end of the experiment. However, there was no significant difference between the HFD and BPS groups (Table 1). SBP was significantly increased in the HFD group compared with the control group. BPS significantly reduced SBP, but SBP in the BPS group was still significantly higher than that in control group (Table 1). HR was significantly increased in the HFD group compared with the control group. BPS reduced HR, but the difference was not statistically significant (Table 1).

After 16 h of fasting, lipid profile and glucose and insulin levels were determined. Total cholesterol and triglyceride were significantly increased by the HFD (Table 2). BPS treatment modestly decreased total cholesterol and triglyceride levels. However, the differences were not statistically significant. Fasting insulin and glucose levels were elevated in the HFD group.

BPS improved GTT and ITT

At the end of experiment, GTTs and ITTs were performed. The HFD group developed glucose intolerance (Fig. 1A) and insulin resistance (Fig. 1C). Treatment of mice with BPS significantly improved glucose tolerance and insulin action (Fig. 1A and C). Interestingly, the basal glucose level was significantly lower in the BPS group compared with the HFD group after 6 h of fasting, which was not observed after 16 h of fasting (Table 2). Area under the curves (AUC) also showed improvement of glucose metabolism by BPS treatment (Fig. 1B and D).

Table 1 BW, SBP, and HR

	BW (g)	**SBP** (mmHg)	**HR** (b.p.m.)
Control ($n=5$)	26·9±0·5	97±3	448±31
HFD ($n=10$)	43·4±1·1†	114±2†	532±15†
HFD+BPS ($n=10$)	43·9±0·9†	106±2*,‡	496±15

HFD, high-fat diet; BPS, beraprost sodium; BW, body weight; SBP, systolic blood pressure; HR, heart rate. $^{*}P<0{\cdot}05$, $^{\dagger}P<0{\cdot}01$ vs control. $^{\ddagger}P<0{\cdot}05$ vs HFD group.

Table 2 Fasting serum chemistry of control, HFD-, and BPS-treated mice

	TC (mg/ml)	**TG** (mg/ml)	**Insulin** (ng/ml)	**Glucose** (mg/ml)
Control ($n=5$)	55±4	66±12	0·16±0·05	59·6±2·6
HFD ($n=10$)	209±9†	94±9*	3·75±0·51†	142·4±7·3†
HFD+BPS ($n=10$)	182±14†	74±6	4·12±0·90†	132·8±6·2†

HFD, high-fat diet; BPS, beraprost sodium; TC, total cholesterol; TG, triglyceride. $^{*}P<0{\cdot}05$ and $^{\dagger}P<0{\cdot}01$ vs control.

BPS reduced adipocyte size

Histological analysis of epididymal WAT showed that the adipocyte size was increased in the HFD group compared with the control group (Fig. 2A and B). Treatment with BPS reduced adipocyte size (Fig. 2C). Statistical analysis confirmed that BPS significantly reduced adipocyte size (Fig. 2D). These data suggest that BPS enhanced adipocyte differentiation. We therefore examined expression of genes related to adipocyte differentiation. *Pparγ* was significantly suppressed by the HFD, which was reversed by BPS (Fig. 3A). The upregulation of *Pparγ* by BPS showed a borderline significance ($P=0{\cdot}06$) when three groups were considered. However, the difference between the HFD and BPS groups was statistically significant if only the HFD groups were compared ($P=0{\cdot}02$). We failed to see a significant effect of BPS treatment on the expression of C/EBPα (Fig. 3B) or adiponectin (Fig. 3C). Although adiponectin mRNA levels were not changed in the three groups, serum adiponectin levels were mildly decreased in the HFD group and BPS groups (Fig. 3D). However, the difference in serum adiponectin levels between the three groups was not statistically significant.

BPS reduced inflammatory changes in WAT in HFD-fed mice

Chronic inflammation in WAT is a common feature of obesity. Therefore, we examined the infiltration of macrophages into adipose tissue. The number of MAC3-positive macrophage aggregation surrounding adipocytes, often referred to as a crown-like structure (CLS) in WAT (Weisberg *et al.* 2003, Xu *et al.* 2003), was significantly increased in the HFD group compared with the control group (Fig. 2E and F; arrowheads). In the control group (Fig. 2E), almost no CLS was observed in WAT. Treatment with BPS significantly decreased the number of CLSs in WAT (Fig. 2G and H).